Helmholtz-Zentrum
hereon

Final Draft
of the original manuscript

Mnasri, N.; Sassi, W.; Msaadi, R.; Serdechnova, M.; Blawert, C.; Ammar, S.:

Emergent α- corundum nano-Al2O3 material for Eriochrome Black T removal.

In: Emergent Materials. Vol. 7, 3 (2024), 973–986.

First published online by Springer Nature: 09.01.2024

http://dx.doi.org/10.1007/s42247-023-00623-8

Emergent α- corundum nano-Al_2O_3 material for Black Eriochrome T removal: Study of the photocatalytic property during the Batch Adsorption process

Nourhen Mnasri [1], Wafa Sassi [1,*], Maria Serdechnova [2],
Carsten Blawert [2], Salah Ammar [1], Jean-Yves Hihn [3]

[1] Faculté des Sciences, Unité de Recherche Électrochimie, Matériaux et Environnement UREME (UR17ES45), Université de Gabès, 6000, Gabès, Tunisia

[2] Institute of Surface Science, Helmholtz-Zentrum Hereon, Max-Planck Strasse 1, 21502 Geesthacht, Germany

[3] Institut UTINAM, CNRS UMR 6213, Univ Bourgogne Franche-Comté, 16 route de Gray, 25030 Besançon Cedex, France

Abstract

The removal of Black Eriochrome T (BET) from aqueous solutions by Al_2O_3 nanoparticles has been investigated as a function of contact time, initial BET concentration, and temperature. The experimental design method generated optimum conditions as t_c = 40 min, 55 mg/L, and T = 298 K. The kinetics study was discussed using different kinetic models: Pseudo-first order (PFO), pseudo-second order (PSO), intraparticle diffusion (IPD), and Elovich model. The adsorption experiments of BET show a better fit to the model pseudo second order (R^2=0.999). The experimental data were analyzed by different isotherm models: Langmuir, Freundlich, Temkin and Dubinin-Radushkevich. Freundlich's well-fitted modeling proved that the adsorption of BET on Alumine occurred as multilayers and on a heterogeneous surface. The Thermodynamic study for the present process was performed by determining the values of ΔG°, ΔH°, and ΔS° indicate that the adsorption was spontaneous, physisorption and exothermic.

Keywords: CCD model; Al_2O_3; Black Eriochorme T; Batch adsorption; Photocatalysis.

* Corresponding author. Tel. : +216 22 58 75 58; Fax: +216 75 300 417

* E-mail address: wafa_icai@yahoo.fr (Wafa Sassi)

* ORCID : 0000-0001-9484-0083

1. Introduction

The increased levels of industrial production have led to a greater demand for synthetic dyes, particularly Azo dyes like Eriochrome Black T (BET). These dyes, known for their carcinogenic and mutagenic properties, pose significant health risks to humans, including symptoms such as migraines, thyroid cancer, asthma, blurred vision, itching, and eczema. They also have adverse effects on animal organisms [1]. The UV–Vis absorption spectrum of BET dye exhibits two distinct absorption peaks. The first, at 615 nm, corresponds to the dye's chromophore compound responsible for its color, while the second, at 240 nm, is linked to the dye's aromatic region. These characteristics are typical of Azo dyes [2]. Numerous studies in the literature aim to address the need for alternative technologies to mineralize BET, as approximately 15% of the dye persists in industrial effluents. This dye is resistant to oxidation, making its removal challenging in conventional water treatment processes [3]. Adsorption/Oxidation process (ADOX) encompass a range of promising technologies for degrading and mineralizing organic compounds. One part of this technology is the heterogeneous photocatalysis, which involves using a semiconductor activated by an energy source, typically light. This activation initiates a series of redox reactions that produce oxidizing species, primarily the hydroxyl radical (HO•). These radicals have the ability to oxidize many recalcitrant organic compounds, ultimately converting them into non-toxic substances like CO_2 and H_2O [3–5]. Common semiconductors studied extensively in heterogeneous photocatalysis include TiO2 and ZnO due to their chemical, thermal, and mechanical stability, affordability, and non-toxic nature [6–8]. Another semiconductor with similar attributes and intriguing photocatalytic properties is Alumina Nanoparticles (Al_2O_3). In fact, aluminum (Al) is one of the most abundant elements in the Earth's crust, and aluminum oxide (Al_2O_3), commonly known as alumina, is a naturally occurring compound that is abundant as well in Tunisia. We may find aluminum oxide in Tunisia as Natural Minerals and/or Bauxite deposits [9–11]. However, this material in its raw form has band gaps exceeding 3.0 eV, limiting their efficiency in generating oxidizing species when exposed to ultraviolet light [12–17]. To expand the absorption of light and improve the efficiency and stability of Alumina nanoparticles in generating oxidizing species ADOX, an alternative approach involves their synthesis in special way known as the Sol/Gel/flocculation route offers the corundum phase and then offers advantages such as reduced time and low energy consumption, making it an appealing approach in material development [18–20].

Given that the use of semiconductors in suspension associated with ADOX process, is a real challenge because it complicates subsequent processes, recycling, and the reutilization of photocatalysts in future treatments, the aim is this study presents a novel Sol-gel/flocculation route to synthesize the α-Al_2O_3 phase photocatalyst, and the optimization of its adsorption and photocatalytic activities under visible light for the degradation of the Azo dye BET. This approach holds promise as an alternative method in the development of effective degradation techniques for this particular substance.

2. Experimental conditions

2.1. α-Al_2O_3 corundum phase

Following the methodology inspired by Rivero et al. [21], 0.156 moles of aluminum chloride ($AlCl_3$) powder, dissolved in 170 ml of 1.5 M hydrochloric acid, are poured into a 5 L beaker containing 0.312 moles of acetone diluted in water. The system is subjected to oxygen bombardment for 2 hours. The oxide is precipitated by rapidly adding 300 ml of ammonia with vigorous stirring at room temperature. After settling, flocculates of alumina appear at the bottom, and the supernatant is removed. To create nanoparticle pieces, flocs were formed by uniaxially pressing the material at 70 MPa, followed by cold isostatic pressing at 275 MPa. Finally, the green bodies were subjected to calcination at 750 ◦C for 2 hours. Finally, in order to remove acetone and ammonia, drying/washing cycles are applied. After drying, the nanoparticles are soaked in distilled water with agitation, then filtered and dried. The process is halted only when the washing water (filtrate) reaches a neutral pH (7). Subsequently, the product undergoes a decreasing sieving process. We stop when all the powder passes through, resulting in nanoparticles of the same size.

The Figure 1 shows the SEM and XRD of dried Al_2O_3 nanoparticles.

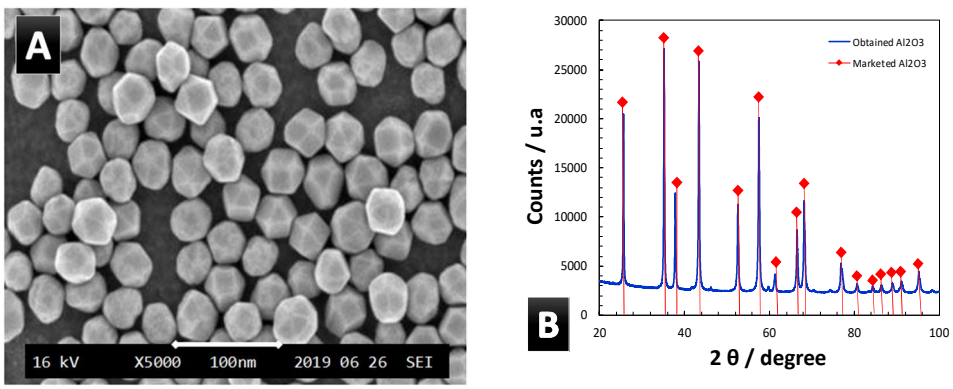

Figure 1: (A): SEM micrograph and (B): DRX diffractogram of dried nano-Al_2O_3

We can observe in Fig.1-A that the nanoparticles are pure, crystalline, and nearly uniform in size. On the other hand, it is possible to observe in Fig.1-B a good correspondence between the main peaks obtained for the final product of prepared nanoparticles and those of the reference diffractogram of α-Al_2O_3 overlaid in red on the figure, confirming the purity of the synthesized corundum phase.

The determination of Alumina pH_{pzc} is carried out using the technique reported by Sassi et al. [22]. To do this, 12 reference solutions of NaCl 0.01 mol/L with pH values ranging from 1 to 12 are prepared. Then, the pH values of each of these solutions are accurately determined. Afterward, 0.6 g of Al_2O_3 is added. The resulting suspensions are left to agitate for 24 hours at room temperature. Finally, their final pH values are measured.

2.2. Adsorbent preparation

All the experimental solutions were meticulously prepared using distilled water. To assess azo-dye adsorption, we constructed a calibration curve and obtained spectra of BET at a consistent temperature of 293 K, as illustrated in Figure 2. The BET UV absorption demonstrates its peak at λ max = 615 nm, affirming the applicability of the Beer-Lambert law in this context. Additionally, the linear relationship displayed a high regression coefficient of R^2 = 0.9989, which closely approaches unity. This finding suggests the feasibility of quantifying BET content in aqueous solutions at λ max = 615 nm.

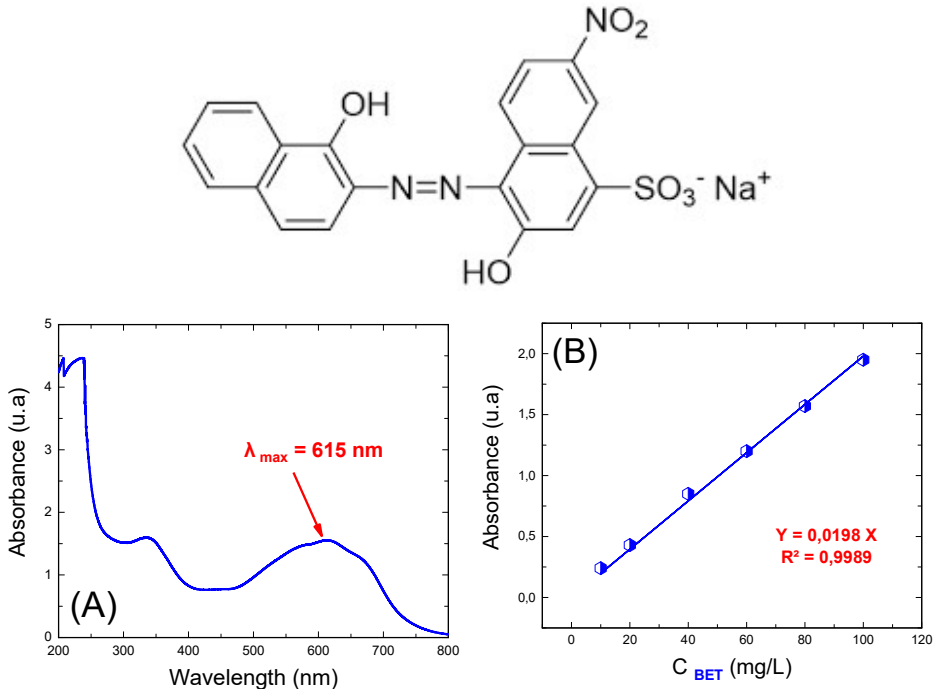

Figure 2: BET molecule structure, (A): UV-Visible spectra and (B): Calibration curve

2.3. Experimental design investigation

The efficiency of removal will be evaluated using the formula mentioned in Eq. (1):

$$Y\ (\%) = \frac{C_{ads}}{C_0} \times 100 \qquad Eq\ (1)$$

The investigation of Black Eriochrome T (BET) adsorption on α-Al_2O_3 nanoparticles involved modeling through a comprehensive composite plan, and for optimization, the Central Composite Design (CCD) was employed. The data were analyzed using STATISTICA software, and the CCD model yielded the predictive equation shown below (Eq. 2):

$$Y = a_0 + a_1x_1 + a_2x_2 + a_3x_3 + a_{12}x_1x_2 + a_{13}x_1x_3 + a_{23}x_2x_3 + \Delta y \qquad Eq\ (2)$$

Where;

Y represents the adsorption yield (%), a_0 stands for the dominant average of the adsorption yield, a_i refers to the first-order coefficient of each factor "i" affecting the adsorption yield, a_{ii} and a_{ij} represent the second-order coefficients of each factor "i" and the interaction effect between factors "i" and "j" on the adsorption yield, respectively. Moreover, ΔY represents the residual error between the predicted and experimental adsorption yield responses.

To select the appropriate kinetic and isotherm models, we assessed Person's Chi-square statistic (χ^2) and the residual sum of squares (RSS) using equations (Eq.3) and (Eq.4), respectively:

$$X^2 = \frac{Y_i - f(x_i, \widehat{\theta})}{\sigma_i} \qquad Eq\ (3)$$

$$RSS\ (X, \hat{\theta}) = \sum_{i=1}^{n} [Y_i - f'(x_i, \hat{\theta})]^2 \qquad Eq\ (4)$$

Here, Y represents the overarching non-linear model, Xi denotes the set of independent variables, and θi signifies the parameter array.

2.4. Instrumentations and techniques

The use of a scanning electron microscope (SEM) enabled the acquisition of high-resolution images depicting the sample's surface by utilizing interactions between electrons and matter. In this investigation, both the initial nanoparticles' samples and those after adsorption underwent equivalent treatment procedures. This involved immersion in aqueous solutions under carefully optimized conditions, including factors like pH, contact duration, initial concentration, and

temperature. Subsequently, FTIR spectra were generated over a wavelength range of 400 to 4000 cm^{-1}. Additional comprehensive details can be found in prior scholarly works [22].

3. Results and discussion

3.1. pH of zero-point charge (pHzc)

The Figure 3 shows the superficial pH evolution.

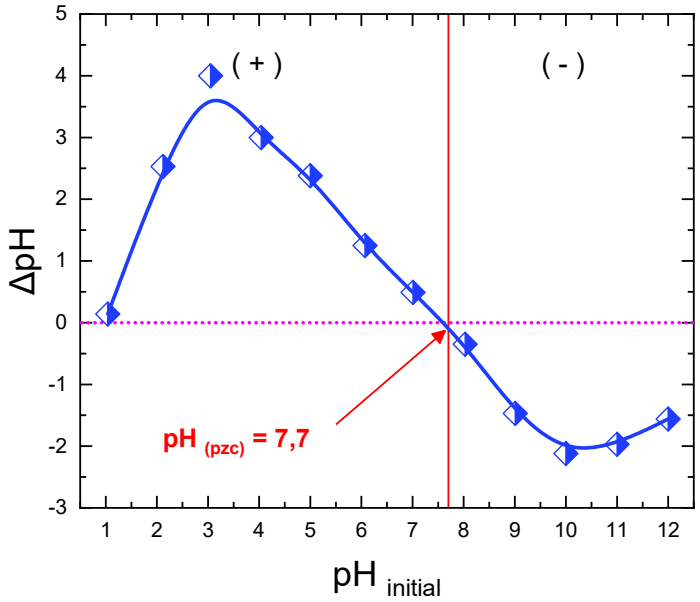

Figure 3: Material's pH values evolution function of media's pH

According to the Figure 3, we can deduce that:

- ✓ pH pzc = 7.7
- ✓ pH < pH pzc = 7.7: The surface of alumina is positively charged.
- ✓ pH > pH pzc = 7.7: The surface of alumina is negatively charged.

In this study, the EBT dye is an anionic compound. Therefore, the pH for the upcoming experiments will be set to an acidic pH where the adsorption rate is maximum. Figure 3 shows that the pH at which the alumina surface is charged with the highest number of positive sites is at pH = 3.5. Therefore, we have chosen to work at a pH adjusted to 3.5 for EBT removal.

3.2. Composite experimental design investigation of BET removal by α-Al_2O_3

In order to gather information on the factors influencing BET removal using Alumina, we conducted an experimental design method using STATISTICA. Optimization was achieved

using the Central Composite Design model (CCD). Table 1 presents the experimental range of the studied factors

Table 1: Experimental range of the studied factors

Factors	Code	-α	(-1)	(0)	(+1)	+α
Contact time t (min)	X_1	5	30	75	120	150
Concentration C_{OTC} (mg/L)	X_2	6	30	65	100	200
Temperature T (K)	X_3	293	303	318	333	343

We utilized the STATISTICA software to implement our experimental design methodology. The optimization of the experiment design was achieved by employing the Central Composite Design (CCD) matrix, which allowed us to investigate the interrelationships between the variables and their effects on BET removal. Figure 4 depicted the obtained optimal conditions.

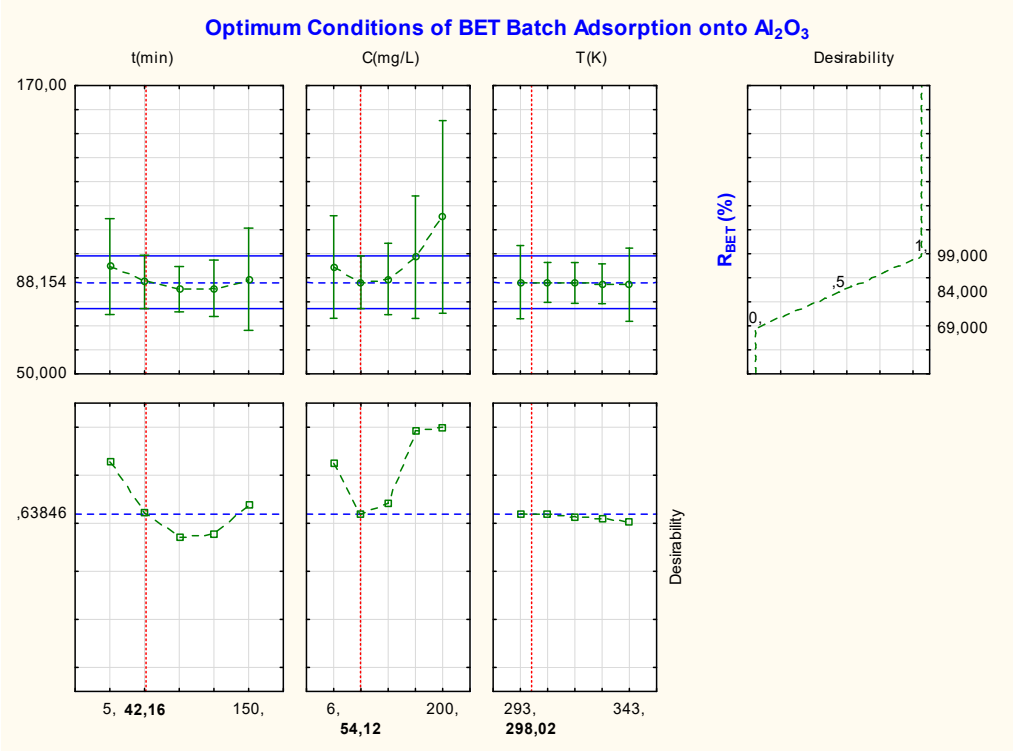

Figure 4 : CCD-STATISTICA conditions generated as optimized for the BET removal by nano-Al_2O_3 (pH =3.5)

Figure 4 provides insight into the adsorption efficiencies of BET on α-Alumina phase, which varies within the range of 69 % to 99 %. This observation underscores the substantial impact of three key factors: contact time, BET concentration, and temperature, as well as the judicious

selection of their experimental ranges. Drawing conclusions based on the optimal conditions depicted in Figure 4:

- ✓ When the desirability is set to 0, the adsorption efficiency is 69 %.
- ✓ A desirability of 0.5 corresponds to an adsorption efficiency of 84 %.
- ✓ A desirability of 1 corresponds to the highest adsorption efficiency at 99 %.

The apply of CCD model leads to the generation of the following prediction equation:

$$Y = 84 - 6.40\,x_1 + 0.51x_2 - 2.35x_3 - 0.22x_1x_2 - 0.17x_1x_3 - 0.18x_2x_3 + 0.5 \qquad Eq\ (5)$$

The reading of Eq.5 proposes the following interpretations:

- ✓ $|a_1| = 6.40 > |a_2| = 0.51$: Contact time has more influence than the initial concentration of BET on removal yield.
- ✓ $|a_1| = 6.40 > |a_3| = 2.35$: Contact time has also more influence than temperature on BET adsorption yield.
- ✓ $|a_2| = 0.51 < |a_3| = 2.35$: The initial concentration of BET has less influence than temperature on BET removal yield.
- ✓ $|a_1| > |a_3| > |a_2|$: Contact time appears to be the significant factor.
- ✓ $a_1 < 0$: The contact time effect is inversely proportional to BET removal yield.
- ✓ $a_2 > 0$: The effect of the BET initial concentration is directly proportional to removal yield.
- ✓ $a_3 < 0$: The effect of temperature is inversely proportional to removal yield.
- ✓ a_{12} , a_{13} , $a_{23} < \Delta y = 2\%$: All interaction effects were lower than the residual Δy indicating that no significant interaction is detected.

Figure 5 illustrates the representation of observed and simulated data in the model.

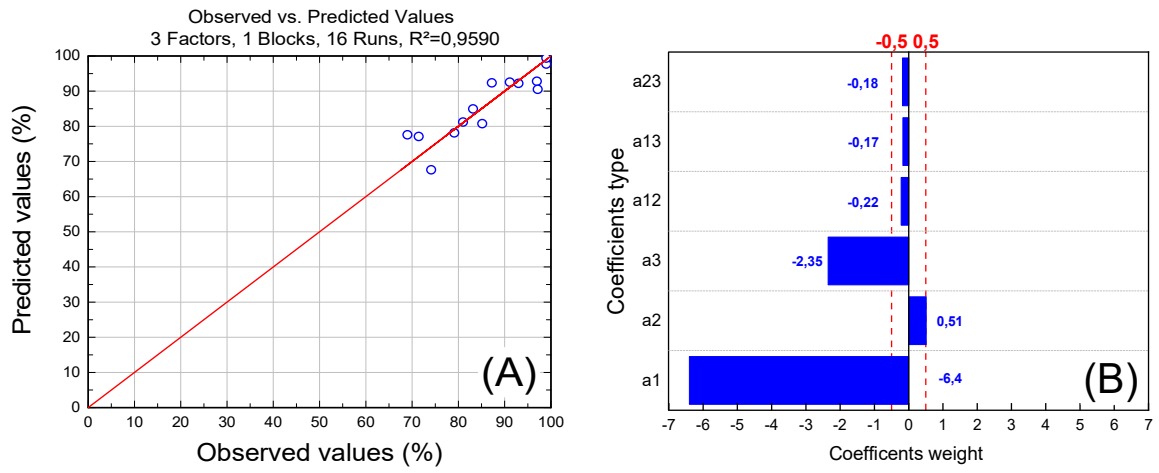

Figure 5 : (A) : Simulation of the experimental data and (B) : Factors effect investigation during BET adsorption onto Al_2O_3 (pH = 3.5)

In accordance with the findings in Figure 5-A, it is evident that the experimental data closely align with the theoretical line. This observation underscores a strong concurrence between the predicted theoretical values derived from Equation (Eq.5) and the actual experimental results, a relationship further supported by the high regression coefficient R^2, nearing unity (R^2=0.9590). This outcome validates the suitability of the CCD model not only for simulating BET adsorption on α-Al_2O_3 nanoparticles but also for the wise selection of the experimental factors involved.

Moving to Figure 5-B, it becomes apparent that a_1 and a_3 exhibit an inversely proportional relationship, whereas a_2 shows a direct relationship with BET adsorption yield. This indicates that media temperature is likely the dominant factor. In contrast, the values of interaction effects (a_{12}, a_{13}, and a_{23}) fall below the Pareto coefficient (or residual uncertainty), which is set at ±0.5. This suggests that no significant interactions are influencing the BET adsorption process onto Alumina. To delve deeper into the mechanism of BET adsorption onto corundum phase, various kinetic and isotherm models were applied. The optimum conditions generated by the CCD model were 42 min, 55 mg/L and 298 K for the contact time, BET initial concentration and bath Temperature, respectively. Under these optimal conditions and at a pH of 3.5, the maximum yield is approximately 99,43%. These values remain constant throughout the rest of the study. The newly introduced parameter for assessing BET adsorption will be denoted as Q, representing the adsorption capacity expressed in mg/g, and its calculation is as follows:

$$Q\ (mg/g) = \frac{C_{ads}}{C_0} \times \frac{V}{m} \qquad Eq\ (6)$$

3.3. SEM characterization of Al_2O_3 before and after BET adsorption

In order to investigate the Alumina nanoparticles morphology, SEM and EDAX cartography were used. The SEM and EDAX map were presented in the Figure 6 before and after the BET removal.

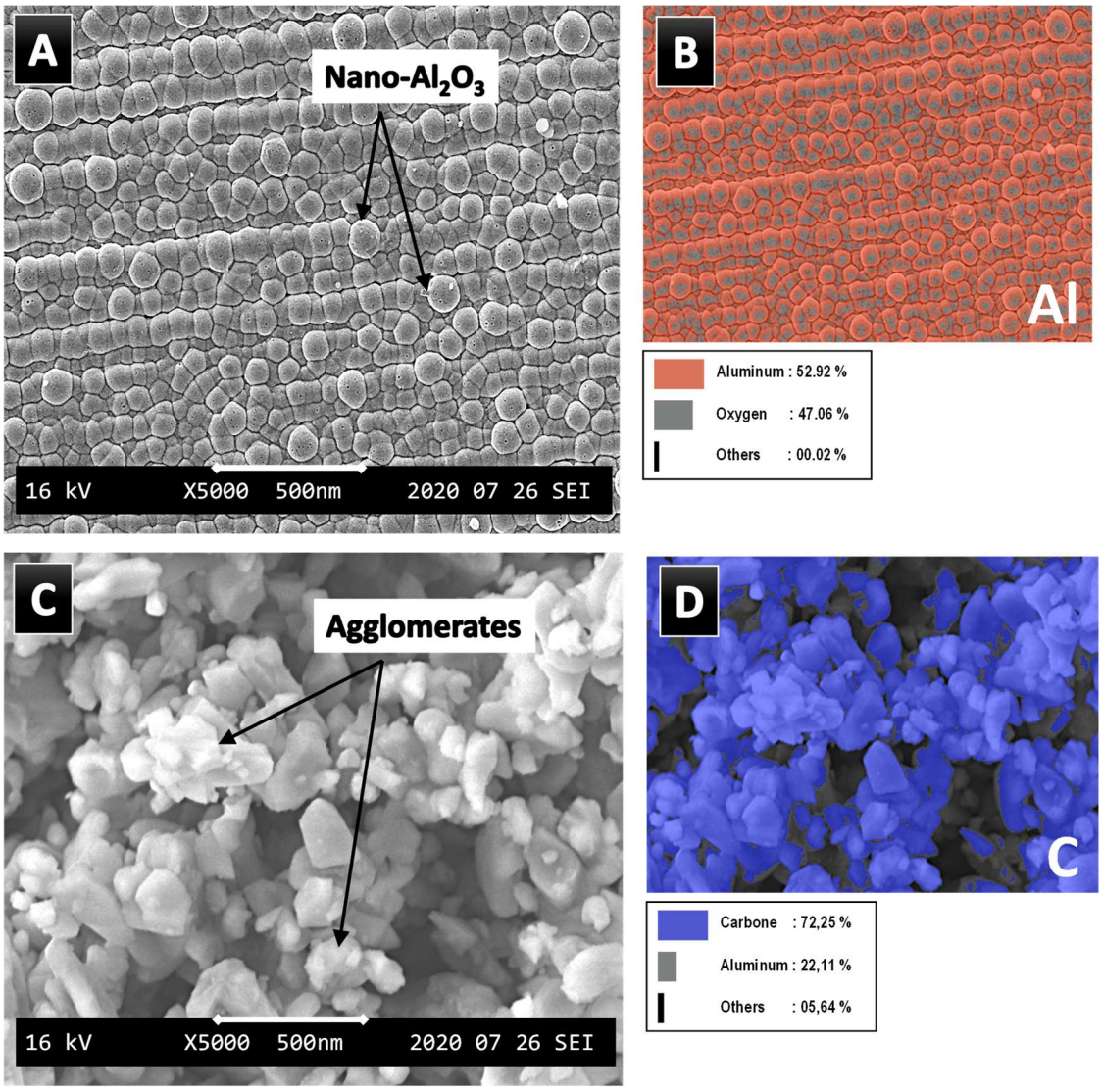

Figure 6 : (A) : SEM micrographs and (B) : FTIR spectra Perlite before and after OTC adsorption at the optimum conditions (pH =3.5, t = 113 min, C = 178 mg/L, and T = 298 K).

Figure 6-A visually depicts the clearly defined borders of Al_2O_3 nanoparticles. Prior to BET adsorption, these nanoparticles appear to exhibit a homogeneous spatial arrangement and geometry. However, it's important to note that this SEM image differs from the micrograph in Figure 1-A. In fact, the dried nanoparticles were found to be dispersed throughout the space, signifying their high degree of crystallinity [21]. The EDAX map in Figure 6-B shows a

majority presence of 53 % and 47 % for Al and O, respectively. This result proves the adsorbent purity as mentioned above.

3.4. Kinetic and Isotherm analysis

In order to investigate the kinetic reaction and adsorption mechanism during BET removal using nano-Al_2O_3, two kinetic studies have been conducted, namely the Pseudo-First Order and the Pseudo-Second Order known as PFO and PSO, respectively. The Eq.7 and Eq.8 present the non-linear models [23,24].

$$Q_t = Q_e \times (1 - e^{-k_{PFO} \times t}) \qquad Eq\ (7)$$

$$Q_t = \frac{k_{PSO} \times Q_e^2 \times t}{1 + k_{PSO} \times Q_e \times t} \qquad Eq\ (8)$$

Where Q_e and Q_t : Represent the equilibrium and at time t of adsorption quantity (mg/g). t: Represents the time (min). k_1 and k_2: Represent the model constant for the PFO and PSO models, respectively. Otherwise, Králik [25] and Crini [26] proposed Langmuir and Freundlich non-linear forms are Eq.9 and 10, respectively:

$$Q_e = \frac{Q_m \times k_L \times C_e}{1 + k_L \times C_e} \qquad Eq\ (9)$$

$$Q_e = k_F \times (C_e)^n \qquad Eq\ (10)$$

Where, C_e: Represents the BET equilibrium concentration (mg/L). Q_e and Q_m: are the equilibrium and theoretical maximum adsorption capacities, respectively (mg/g). k_L and k_F: Represent the Langmuir and Freundlich constants (L/mg), respectively. n: estimates the number of adsorbed BET multilayers onto the material [27].

Figure 7 displays the empirical representation of PFO, PSO, Langmuir and Freundlich modeling of the BET adsorption capacities onto nano-alumina function of time (min) and BET content (mg/L), respectively. Table 2 presented the model parameters.

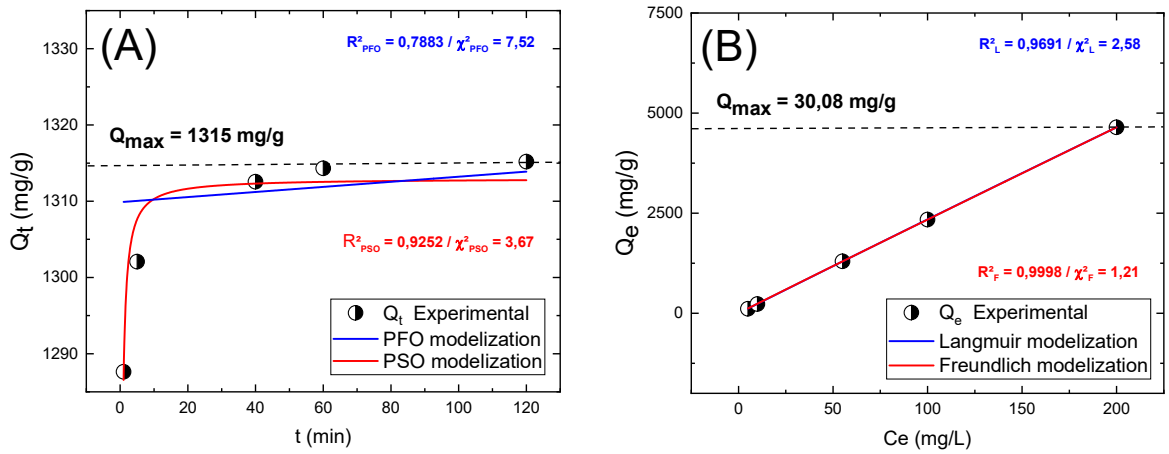

Figure 7 : Experimental, (A) : Kinetic and (B) : Isotherm non- linear modelizations of the BET adsorption onto nano-Al_2O_3 (pH = 3.5, C = 178 mg/L, and T = 298 K).

Table 2 : Kinetic and isotherms modelization parameters of BET adsorption onto α- corundum nano-Al_2O_3

Pseudo-First-Order (PFO)			Pseudo-Second-Order (PSO)		
k_{PFO} (min^{-1})	Q_e (mg/g)	R^2	k_{PSO} (mg/g. min)	Q_e (mg/g)	R^2
0.14	1280.12	0.7883	0.011	1310.01	0.9252
Langmuir			Freundlich		
k_L (min^{-1})	Q_{max} (mg/g)	R^2	k_F ($mg/g^{-1} L^{1/n}$)	n	R^2
0.002	100.05	0.9691	1.414	7.168	0.9998

From the curve, it can be observed that the adsorption of BET on alumina follows a rapid kinetic process. Indeed, the adsorption rate begins with a linear jump of approximately 25 minutes. Furthermore, saturation is observed starting at around 50 minutes and stabilizes around 120 minutes, where Q_{max} equals 1315 mg/g. This value is very close to the adsorption capacity obtained under optimal conditions, which is 1312.584 mg/g.

The results obtained in the Figure 7-A show that the regression coefficient R^2 is equal to 0.78. This means that the adsorption kinetics do not conform to the PPO model. In fact, the obtained simulation was line with positive slope. According to the Figure 7-A, it is noticeable that the regression coefficient R^2 is equal to 0.92. This value is very close to unity. This indicates that the adsorption kinetics of BET appear to conform to the pseudo-second-order model (PSO).

In Figure 7-A, the obtained plot results in a good simulation curve to the experimental points. The theoretical value of the adsorbed quantity, Q_e = 1310 mg/g, is close to the experimental Qe, which is equal to 1315 mg/g. This suggests that the reaction rate depends not only on the adsorption capacity of alumina but also on the concentration of the dye BET [28,29].

In the Langmuir isotherm study (Figure 7-B), the regression coefficient is equal to 0.96. To determine the feasibility of adsorption, the dimensionless constant R_L is calculated using the following relationship [30]:

$$R_L = \frac{1}{1+K_L \times C_0} \qquad Eq\ (11)$$

As proposed by Langmuir [31], when:

$R_L = 0$: Adsorption is irreversible.

$0 < R_L < 1$: Adsorption is favorable.

$R_L = 1$: Adsorption is linear.

$R_L > 1$: Adsorption is unfavorable.

The Table 3 below presents the different R_L values.

Table 3 : R_L Values for Different BET Concentrations

Concentration EBT	*30*	*55*	*100*	*200*
R_L	*0.424*	*0.286*	*0.180*	*0.099*

The R_L values obtained are all between 0 and 1, indicating that the adsorption process of BET on alumina is favorable.

In the Figure 7. B and Table 2, the Freundlich isotherm constant, 1/n, can be used to calculate the adsorption capacity and explore the favorability of the adsorption process. In cases where the value of n is positive, it can indicate the number of adsorption layers [32]. The regression coefficient R^2 is equal to 0.99. This suggests that the Freundlich model can describe the adsorption mechanism. Therefore, it can be suggested that there is multi-layer adsorption on a heterogeneous surface. Additionally, it appears to be a physically driven adsorption process [33].

3.5. Thermodynamic study

To study the temperature effect on the BET adsorption process on Al_2O_3 nanoparticles, the temperature was varied from 298 to 338 K at pH 3.5. The solution concentration was maintained at 55 mg/L, and the contact time was set at 40 minutes.

Figure 8 illustrates the temperature effect during the BET removal by adsorption on alumina and the modelized Van't Hoff curve. All thermodynamic parameters were gathered in Table 4.

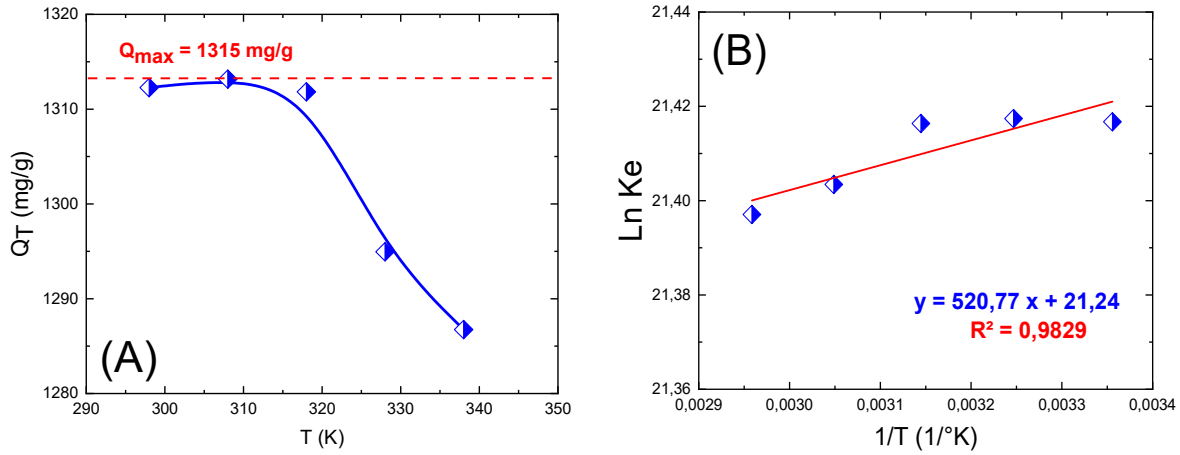

Figure 8 : (A) Evolution of QT function of temperature and (B) :Vant'Hoff straight line of BET adsorption on alumina (pH=3.5, t=40 min, and C_{BET}=55 mg/L)

Table 4: Thermodynamic parameters obtained for BET adsorption onto nano-Al_2O_3

Temperature (K)	ΔG° (kJ mol^{-1})	ΔH° (kJ mol^{-1})	ΔS° (J mol^{-1} K^{-1})
298	-53,099	-4,332	+176,716
308	-54,883		
318	-56,662		
328	-58,409		
338	-60,171		

This Figure 8-A and 8-B illustrates a clear inverse relationship between the adsorption capacity of nano-Al_2O_3 and temperature. Specifically, as the temperature rises, the adsorption capacity (Q_T) decreases. This observation strongly implies that the BET adsorption process on alumina is exothermic, as reported in reference [34]. In Table 4, the negative ΔG° values further support this, indicating the spontaneity of the BET adsorption onto Al_2O_3. Additionally, the positive value of ΔH°, measured at -4.33 kJ/mol, confirms the exothermic nature mentioned earlier. Furthermore, the low enthalpy suggests that physical adsorption of BET onto alumina is the prevailing mechanism. The relatively high entropy value (+176 J/mol in Table 4) provides insight into the significant disorder on the alumina surface, thus confirming the presence of a physisorption process.

3.6. Application on Real Wastewater

In order to assess whether the α-corundum Al_2O_3 nanoparticles adsorb Black Eriochrome T completely when mixed with other dyes, we conducted a test on a real wastewater sample. The wastewater sample was a concentrated 1-liter sample obtained from the ATENA company in Sfax (Tunisia), used in the production of jeans. Given its high concentration and impurity

content, we diluted it by a factor of 100 to enable analysis using UV-Visible spectroscopy. To evaluate the BET efficiency removal by Al_2O_3 nanoparticles in a real wastewater sample, we applied both the normal conditions, the natural pH of the waste (pH 6.8) and optimized conditions derived from the STATISTICA software using a CCD model (pH 3.5). For empiric comparison the contact time was fixed at 40 minutes as suggested by the CCD model for both tests. Figure 9 presents the overlay of UV-Visible spectra along with the adsorption yields obtained under various conditions.

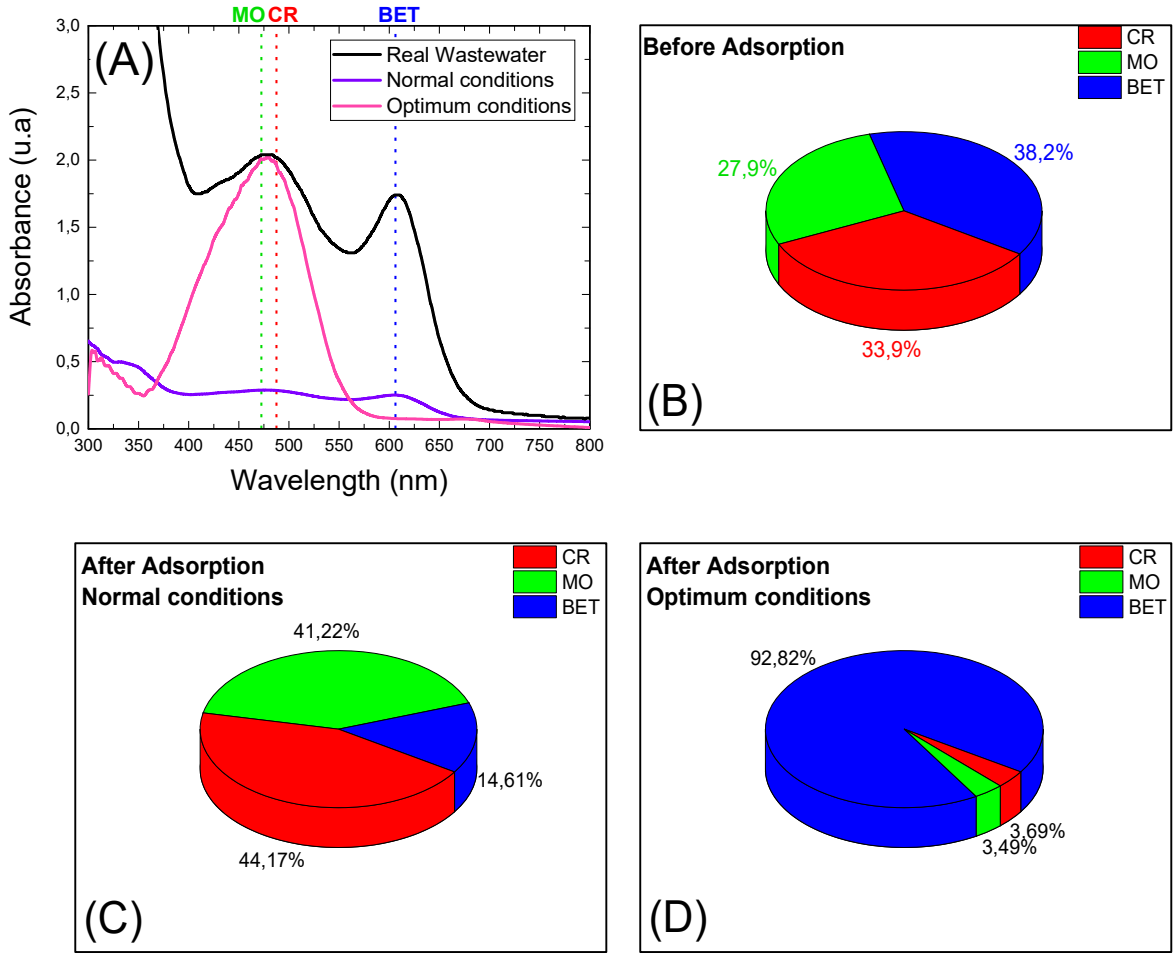

Figure 9 : (A): UV-Visible Spectra and (B): Yields of the real wastewater sample before and after adsorption on nano-Al_2O_3 under normal (pH=6.8) and optimal conditions (pH=3.5) at T=298 K

Firstly, Figure 9-A shows that the wastewater contains Methyl orange (MO), Congo Red (CR) and Black Eriochrome T (BET) referring to their absorbance wavelength 470, 490 and 615 nm, respectively. Moreover, Figure 9-B shows that the dyes contents are equal presenting 33.9, 27.9 and 38.2 %, for the CR, MO and BET, respectively.

Following adsorption on α- corundum nano-Al_2O_3 under normal conditions (pH=6.8) the wastewater spectrum has undergone both qualitative and quantitative changes. Notably, the

peaks corresponding to the Black Eriochrome T dye and other impurities have vanished (Figure 9-A). Furthermore, the adsorption yield of BET under these conditions was 14.61 %. This indicates that Al_2O_3 nanoparticles have succeeded in removing not only BET but also the other dyes present in the wastewater. The removal efficiency was 44.17, 41.22 and 14.61 %, for the CR, MO and BET, respectively. This outcome underscores the simultaneous adsorptive nature of the material under these conditions. Consequently, it confirms the unconditioned affinity of alumina for all dyes present in the wastewater.

In the same Figure 9-A, applying adsorption on α- corundum nano-Al_2O_3 under optimal conditions (pH=3.5, and t=40min) reveals that the spectrum exhibits only peaks related to competitive dyes (MO and CR). The BET peak has completely disappeared, and the removal efficiency reaches 93%. This result demonstrates that under optimal conditions, alumina transforms into a material with selective adsorption capabilities for Black Eriochrome T.

3.7. The α- corundum nano-Al_2O_3 photocatalytic activity

α-corundum nano-Al_2O_3 are semiconductor nanoparticles known for their unique properties. They exhibit a modest level of photocatalytic activity in the presence of solar radiation. These nanoparticles are also recognized for their high thermal stability, excellent chemical resistance, and exceptional hardness. Figure 10 demonstrates the alignment between the solar radiation spectrum and the inherent perlite radiation spectrum.

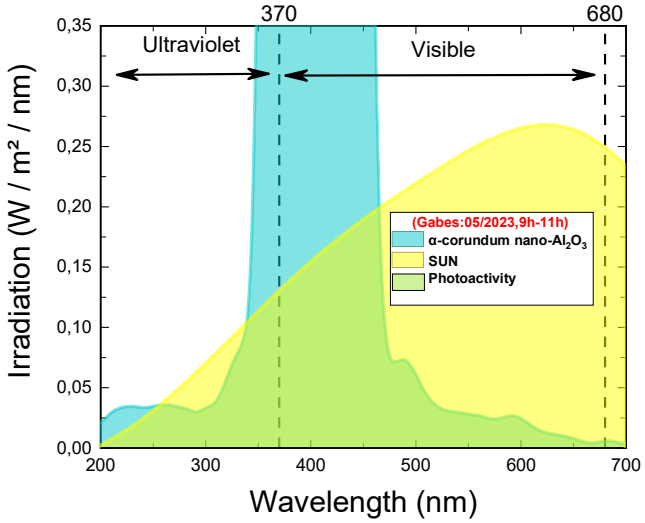

Figure 10 : Photocatalytic activity range of α-corundum nano-Al_2O_3 concerning the average solar radiation spectrum recorded in Gabes-Tunisia during May 2023, between 9 AM and 11 AM

The intersection range (green area) between the two spectra is conspicuously positioned in the visible range, specifically peaking between 320 and 450 nm. To investigate the role of photocatalysis in the treatment of pollutants through Alumina adsorption, we conducted BET

adsorption experiments in three distinct reactors: a dark reactor, a solar reactor, and a reactor exposed to standard laboratory lighting. These tests were carried out under optimized BET adsorption conditions for Al_2O_3 (pH 3.5, 40 minutes, and 55 mg/L). Figure 11 provides an illustration of the alignment between the UV spectra and the BET removal efficiencies observed in the three different reactors.

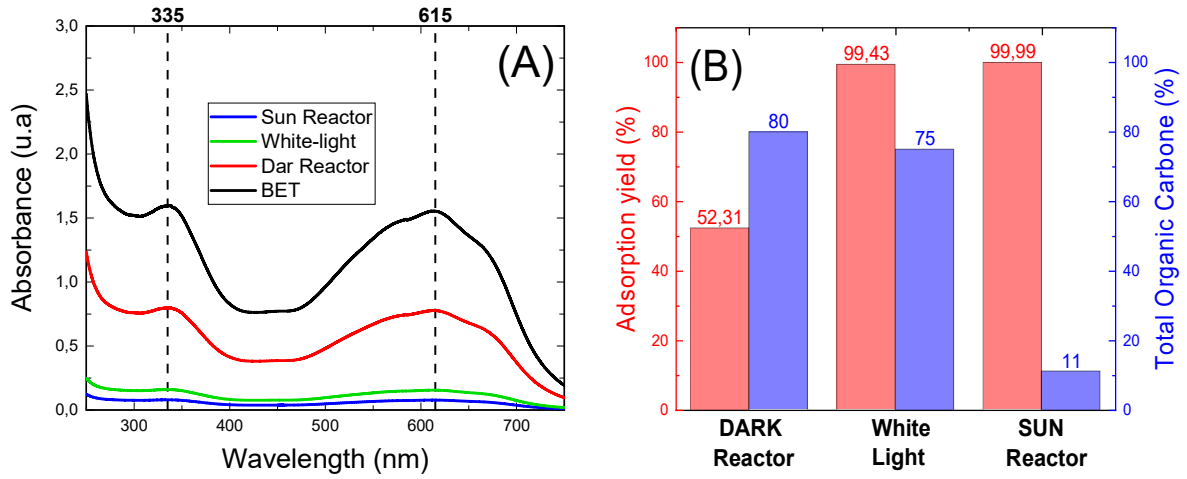

Figure 11 : (A) UV-VISIBLE spectra and (B) Histograms of BET Adsorption/Oxidation efficiencies in the three reactors: Dark, white-Light, and SUN (pH 3.5, 40 minutes, 55 mg/L)

The examination of UV-Visible absorption spectra both before and after BET removal via Alumina reveals distinct characteristic peaks (see Figure 11-A). The first peak, situated at approximately 335 nm, and the second peak, detected around 615 nm, correspond to specific electronic transitions of the BET molecule. Notably, no additional peaks emerged during photosorption, indicating that the BET molecule did not degrade into colored secondary products.

As depicted in Figure 11-B, the efficiency in the dark reactor is notably low at 52.31%. However, conducting the experiment under sunlight radiation significantly boosted efficiency to 99.99%. This outcome underscores that Alumina serves not only as an effective material for batch adsorption but also enhances photosorption. It's important to highlight that the BET removal efficiencies reached 99.43% and 99.99% for the white-light and Sun reactors, respectively. This finding strongly supports the notion that dye removal primarily occurs within the visible light range, as previously suggested in Figure 10.

Conversely, the Total Organic Carbon (TOC) analysis reveals a high percentage of organic carbon remaining in the white-light reactor, approximately 75%. This observation indicates the

non-degradation of BET molecules. The substantial BET removal yield in the white-light reactor can be attributed to the disappearance of the chromophore responsible for the dye's black color and absorption at 615 nm. The use of sunlight, on the other hand, photocatalyzed the BET molecules, leading to a mineralization and then a significant reduction in the Total Organic Carbon percentage to 11%.

4. Conclusion

The objective of this study is to investigate the removal of the Black Eriochrome T dye through adsorption onto α- corundum nano-Al_2O_3. The key findings where firstly, the pH at which the net charge is zero corresponds to 7.7. Secondly, the optimal parameters for BET adsorption on alumina are as follows: pH = 3.5, contact time = 40 minutes, initial BET concentration = 55 mg/L, and optimal temperature = 298 K. Thirdly, kinetic and isotherms studies reveal that BET adsorption follows the Pseudo-Second Order (PPO) and the Freundlich models, indicating a multilayer adsorption process. When thermodynamic analysis indicates that the adsorption is exothermic, spontaneous, and physically driven.

Then, treating real wastewater shows that alumina is selective for BET under the optimal conditions of pH (pH 3.5). However, under normal conditions of pH (pH 6.8), the adsorption remains simultaneous for all constituents, resulting in an increase in efficiency from 14 % to 93%.

Finally, the experiment conducted in direct sunlight conclusively demonstrates a synergistic Adsorption/Oxidation process. This assertion is substantiated by Total Organic Carbon (TOC) analyses, which validate the reduction in the total organic carbon content in the solution following oxidation. These results offer significant insights into not only the adsorption behavior of Black Eriochrome T on α-corundum nano-Al_2O_3 but also the mineralization of the pollutant within the solar reactor and then the reuse of 100% treated wastewater.

5. Acknowledgement

The authors would like to acknowledge the Tunisian Ministry of Higher Education and Scientific Research for generously providing financial support through Project Code (22PEJC-D1P3).

6. Statements and Declarations

6.1. Ethical Approval

Each of the authors purposefully endorsed the ethical guidelines adopted by the journal.

6.2. Consent to Participate

Every author has granted complete and unanimous agreement to partake in the conceptualization and advancement of this research project.

6.3. Consent to Publish

Each author intentionally agrees to the publication of this work.

6.4. Funding

Not applicable.

6.5. Competing Interests

Not applicable.

6.6. Availability of data and materials

No data available.

6.7. Conflict of interest

The corresponding author, speaking on behalf of all the authors, affirms the absence of any conflicts of interest.

7. References

[1] A. Silva Gomes, M. Vitória Guimarães Leal, G. Roefero Tolosa, F. Camargo Cabrera, G. Dognani, A. Eloízo Job, Cationic dialdehyde cellulose microfibers for efficient removal of eriochrome black T from aqueous solution, Bioresour. Technol. 380 (2023) 129096. https://doi.org/10.1016/j.biortech.2023.129096.

[2] S. Riaz, A. Jabbar, Ambreen, S. Khaskheli, S. Sagheer, M.I. Choudhary, Anthraquinone based anti-UV acid-azo dyes; a study of their synthesis, fastness, and UV-protection properties, J. Mol. Struct. 1272 (2023) 134219. https://doi.org/10.1016/j.molstruc.2022.134219.

[3] S. Lu, X. Dong, B. Zhang, Q. Zhou, X. Zhang, Y. Liao, Y. Yang, H. Wang, Colorimetric and fluorescent dual-channel sensor array based on Eriochrome Black T/Eu3+ complex for sensing of multiple tetracyclines, J. Mol. Liq. 351 (2022) 118371. https://doi.org/10.1016/j.molliq.2021.118371.

[4] H. Hajjaoui, A. Soufi, H. Khiar, M. Abdennouri, M. Achak, N. Barka, Preparation of sodium zinc phosphate/polyaniline nanocomposite for Cr(VI) and eriochrome black T adsorption from water, Mater. Today Commun. 36 (2023) 106755. https://doi.org/10.1016/j.mtcomm.2023.106755.

[5] R.H. Waghchaure, V.A. Adole, B.S. Jagdale, Photocatalytic degradation of methylene blue, rhodamine B, methyl orange and Eriochrome black T dyes by modified ZnO nanocatalysts: A concise review, Inorg. Chem. Commun. 143 (2022) 109764. https://doi.org/10.1016/j.inoche.2022.109764.
[6] I. Ghanmi, W. Sassi, P. Oulego, S. Collado, A. Ghorbal, M. Díaz, Optimization and comparison study of adsorption and photosorption processes of mesoporous nano-TiO2 during discoloration of Indigo Carmine dye, Microporous Mesoporous Mater. 342 (2022) 112138. https://doi.org/10.1016/j.micromeso.2022.112138.
[7] C. Anselmi, E. Mosconi, M. Pastore, E. Ronca, F. De Angelis, Adsorption of organic dyes on TiO2 surfaces in dye-sensitized solar cells: interplay of theory and experiment, Phys. Chem. Chem. Phys. 14 (2012) 15963. https://doi.org/10.1039/c2cp43006a.
[8] A. Ashpak Shaikh, M. Rajendra Patil, B. Sonu Jagdale, V. Ashok Adole, Synthesis and characterization of Ag doped ZnO nanomaterial as an effective photocatalyst for photocatalytic degradation of Eriochrome Black T dye and antimicrobial agent, Inorg. Chem. Commun. 151 (2023) 110570. https://doi.org/10.1016/j.inoche.2023.110570.
[9] M.Y. Habibi, B. Samet, Y. El Hafiane, A. Smith, Synthesis and characterization of cement clinker based on Tunisian dam sediments, Constr. Build. Mater. 394 (2023) 132254. https://doi.org/10.1016/j.conbuildmat.2023.132254.
[10] W. Slimene, J. Touir, N. Fatteh, L. Khélil, Z. Saiid, M. Bouzid, Study of the Upper Paleocene-Lower Ypresian phosphate succession in El Guettar out crop (Gafsa area, central Tunisia), J. Afr. Earth Sci. 177 (2021) 104125. https://doi.org/10.1016/j.jafrearsci.2021.104125.
[11] R. Fersi, H. Jabbalah, A. Bezergheanu, D. Patroi, C.B. Cizmas, L. Bessais, N. Mliki, Microstructure and magnetic anisotropy properties of Pr2Co7 films deposited on Al2O3(0001) substrate, Vacuum. 174 (2020) 109168. https://doi.org/10.1016/j.vacuum.2020.109168.
[12] A.K. Kaviti, S.R. Akkala, Influence of anodization time on Al2O3 nanoporous morphology and optical properties using energy band gap at room temperature, Results Eng. 17 (2023) 100816. https://doi.org/10.1016/j.rineng.2022.100816.
[13] K.A. A. Min-Dianey, H. Zhang, N.L.P. M'Bouana, A. Imran, P.V. Pham, X. Xia, Near-infrared transmissive properties of porous Si/Al2O3 photonic crystal band gaps, Mater. Today Commun. 33 (2022) 104323. https://doi.org/10.1016/j.mtcomm.2022.104323.
[14] A.V. Voitsekhovskii, S.N. Nesmelov, S.M. Dzyadukh, V.S. Varavin, S.A. Dvoretsky, N.N. Mikhailov, M.V. Yakushev, G.Y. Sidorov, Electrical characterization of insulator-semiconductor systems based on graded band gap MBE HgCdTe with atomic layer deposited Al2O3 films for infrared detector passivation, Vacuum. 158 (2018) 136–140. https://doi.org/10.1016/j.vacuum.2018.09.054.
[15] E. Barajas-Ledesma, M.L. García-Benjume, I. Espitia-Cabrera, M. Ortiz-Gutiérrez, F.J. Espinoza-Beltrán, J. Mostaghimi, M.E. Contreras-García, Determination of the band gap of TiO2–Al2O3 films as a function of processing parameters, Mater. Sci. Eng. B. 174 (2010) 71–73. https://doi.org/10.1016/j.mseb.2010.05.001.
[16] R.C.R. Santos, E. Longhinotti, V.N. Freire, R.B. Reimberg, E.W.S. Caetano, Elucidating the high-k insulator α-Al2O3 direct/indirect energy band gap type through density functional theory computations, Chem. Phys. Lett. 637 (2015) 172–176. https://doi.org/10.1016/j.cplett.2015.08.004.
[17] C.S. Praveen, V. Timon, M. Valant, Electronic band gaps of ternary corundum solid solutions from Fe2O3–Cr2O3–Al2O3 system for photocatalytic applications: A theoretical study, Comput. Mater. Sci. 55 (2012) 192–198. https://doi.org/10.1016/j.commatsci.2011.11.025.

[18] Y. Zhai, A. Fan, K. Zhong, D.V. Karpinsky, Q. Gao, J. Yi, L. Liu, Great enhancement of ferroelectric properties of Al2O3-modified BiFeO3 thin films obtained by sol-gel method, J. Eur. Ceram. Soc. 44 (2024) 224–232. https://doi.org/10.1016/j.jeurceramsoc.2023.08.058.
[19] W. Sang, X. Yang, H. Tian, J. Wang, Y. Wang, Z. Li, Properties of SiO2-B2O3-Li2O-ZnO-Al2O3 glass-ceramic-coated diamond particles prepared by sol-gel method, Diam. Relat. Mater. 139 (2023) 110392. https://doi.org/10.1016/j.diamond.2023.110392.
[20] R. D.T. Barreto, L. Pereira Ramos, R.M. M. Jorge, L.M. M. Jorge, Turning glycerol surplus into renewable syngas through glycerol steam reforming over a sol-gel Ni–Mo2C-Al2O3 catalyst, Int. J. Hydrog. Energy. 48 (2023) 16614–16629. https://doi.org/10.1016/j.ijhydene.2023.01.166.
[21] P. Rivero-Antúnez, V. Morales-Flórez, F.L. Cumbrera, L. Esquivias, Rietveld analysis and mechanical properties of in situ formed La-β-Al2O3/Al2O3 composites prepared by sol-gel method, Ceram. Int. 48 (2022) 24462–24470. https://doi.org/10.1016/j.ceramint.2022.05.058.
[22] W. Sassi, H. Boubaker, H. Ben-khaled, S. Dhaoui, A. Ghorbal, J.-Y. Hihn, Modelization and implementation of free adsorption and electrosorption of Cr (VI) from wastewater using Al2O3 nanoparticles: assessment and comparison of the two processes, Environ. Sci. Pollut. Res. 28 (2021) 28349–28366. https://doi.org/10.1007/s11356-021-12612-7.
[23] Lagergren, S, About the theory of so-called adsorption of soluble substances., (1898).
[24] S.H. Chien, W.R. Clayton, Application of Elovich Equation to the Kinetics of Phosphate Release and Sorption in Soils, Soil Sci. Soc. Am. J. 44 (1980) 265–268. https://doi.org/10.2136/sssaj1980.03615995004400020013x.
[25] M. Králik, Adsorption, chemisorption, and catalysis, Chem. Pap. 68 (2014). https://doi.org/10.2478/s11696-014-0624-9.
[26] G. Crini, E. Lichtfouse, L. Wilson, N. Morin-Crini, Adsorption-oriented processes using conventional and non-conventional adsorbents for wastewater treatment, in: Green Adsorbents Pollut. Remov., Springer Nature, 2018: pp. 23–71. https://doi.org/10.1007/978-3-319-92111-2_2.
[27] A. Saxena, A.K. Srivastava, A. Sharma, B. Singh, Kinetics of adsorption of 2-chloroethylethylsulphide on Al2O3 nanoparticles with and without impregnants, J. Hazard. Mater. 169 (2009) 419–427. https://doi.org/10.1016/j.jhazmat.2009.03.112.
[28] M. Halanur Mruthunjayappa, C. Shachar, A. Imbar, O.A. Menashe, H. Mamane, Cellulose acetate and polycaprolactone based photoactive ultrafiltration membrane: A novel approach with UV-switchable photocatalytic activity, Sep. Purif. Technol. 329 (2024) 125102. https://doi.org/10.1016/j.seppur.2023.125102.
[29] M. Saood Manzar, T. Ahmad, N. Ullah, P. Velayudhaperumal Chellam, J. John, M. Zubair, R.J. Brandão, L. Meili, O. Alagha, E. Çevik, Comparative adsorption of Eriochrome Black T and Tetracycline by NaOH-modified steel dust: Kinetic and process modeling, Sep. Purif. Technol. 287 (2022) 120559. https://doi.org/10.1016/j.seppur.2022.120559.
[30] R. Sanz, G. Calleja, A. Arencibia, E.S. Sanz-Pérez, Amino functionalized mesostructured SBA-15 silica for CO2 capture: Exploring the relation between the adsorption capacity and the distribution of amino groups by TEM, Microporous Mesoporous Mater. 158 (2012) 309–317. https://doi.org/10.1016/j.micromeso.2012.03.053.
[31] C.S.T. Araújo, I.L.S. Almeida, H.C. Rezende, S.M.L.O. Marcionilio, J.J.L. Léon, T.N. de Matos, Elucidation of mechanism involved in adsorption of Pb(II) onto lobeira fruit (Solanum lycocarpum) using Langmuir, Freundlich and Temkin isotherms, Microchem. J. 137 (2018) 348–354. https://doi.org/10.1016/j.microc.2017.11.009.

[32] F.O. Erdogan, Freundlich, Langmuir, Temkin, DR and Harkins-Jura Isotherm Studies on the Adsorption of CO2 on Various Porous Adsorbents, Int. J. Chem. React. Eng. 17 (2019). https://doi.org/10.1515/ijcre-2018-0134.
[33] T.B.N. Pham, H.T.T. Ngoc, S.T. Dinh, N.T.L. Tan, T.L.N. Phuc, T.P. Mai, D.Q. Nguyen, Synthesis of Ferromagnetic Nanocomposites from Nanocrystalline Cellulose and Characterization as an Adsorbent to Remove Lead in the Water, In Review, 2023. https://doi.org/10.21203/rs.3.rs-2639545/v1.
[34] Z. Cui, J. Wen, J. Chen, Y. Xue, Y. Feng, H. Duan, B. Ji, R. Li, Diameter dependent thermodynamics of adsorption on nanowires: A theoretical and experimental study, Chem. Eng. Sci. 247 (2022) 117061. https://doi.org/10.1016/j.ces.2021.117061.